

Asymmetric dark matter from leptogenesis in type-III seesaw framework with modular S_4 symmetry

Abhishek^{1,*}, V. Suryanarayana Mummidi^{1,†}

¹*Department of Physics, National Institute of Technology,
Tiruchirappalli-620015, India*

E-mail: 413120051@nitt.edu, venkata@nitt.edu

ABSTRACT: We present a unified framework for neutrino masses, baryogenesis, and dark matter based on a modular S_4 symmetry combined with a type-III seesaw mechanism. All Yukawa couplings, CP phases, and flavor textures originate from a single complex modulus τ , whose vacuum expectation value controls both visible and dark sector dynamics. The same modular parameter fixes the neutrino mass matrix, determines the CP asymmetries driving resonant leptogenesis, and correlates the resulting baryon and dark matter abundances. A detailed numerical analysis shows that the model reproduces all neutrino oscillation data within the 3σ NuFIT 5.2 (2024) ranges for normal ordering, predicting $\delta_{\text{CP}} \simeq \pm(150^\circ - 180^\circ)$, $\sum m_\nu \simeq (0.06 - 0.08)$ eV, and an effective Majorana mass $m_{\beta\beta} \simeq (8 - 18) \times 10^{-3}$ eV, testable in next-generation neutrinoless double-beta decay experiments. The same modular Yukawas yield resonantly enhanced CP asymmetries $|\epsilon_{L,\chi}| \sim 10^{-9} - 10^{-6}$ at $M_\Sigma \sim 10^7$ GeV, successfully generating the observed baryon asymmetry $\eta_B \simeq 6 \times 10^{-10}$ and dark relic density $\Omega_\chi h^2 \simeq 0.12$ without additional free parameters. The predicted correlation $\Omega_\chi/\Omega_B \simeq 5.4$ fixes the dark matter mass to $m_\chi \simeq 0.1 - 2$ GeV, consistent with all current constraints. This framework therefore realizes a fully predictive baryon–dark matter co-genesis, where the geometry of the modular symmetry links the origin of flavor, CP violation, and the cosmic matter asymmetry.

Contents

1	Introduction	2
2	Model	4
3	Leptogenesis and Asymmetric Dark Matter	7
3.1	Co-genesis framework	7
3.2	Resonant CP asymmetries	7
3.3	Decay widths and branching ratios	8
3.4	Boltzmann evolution	9
3.5	Relic asymmetries and dark matter abundance	9
4	Numerical Analysis	10
4.1	Neutrino Sector	10
4.2	Baryon–Dark Matter Co-genesis	14
4.3	Correlation between CP Asymmetries and Relic Densities	17
4.4	Dependence on Dark Matter Mass and Benchmark Predictions	18
5	Conclusion	20
Appendix A: Essentials of Modular Symmetry and S_4 Yukawa Multiplets		21
Appendix B: Standard Parameterization of Neutrino Observables		23
Appendix C: Boltzmann Framework and Scattering Integrals		23
Appendix D: Dependence on the Dark Yukawa Coupling y_{DM}		24

1 Introduction

Neutrino physics continues to challenge the completeness of the Standard Model (SM) by revealing phenomena that cannot be accommodated within its original structure. The discovery of neutrino oscillations by Super-Kamiokande [1], SNO [2], and KamLAND [3] firmly established that neutrinos possess tiny but nonzero masses, requiring new degrees of freedom beyond the SM. At the same time, cosmological observations from Planck 2018 [4] and DESI 2024 [5] determine the baryon and dark matter relic densities with high precision,

$$\Omega_B h^2 = 0.0224 \pm 0.0001, \quad \Omega_\chi h^2 = 0.120 \pm 0.001, \quad (1.1)$$

yielding the striking ratio $\Omega_\chi/\Omega_B \simeq 5.4$. The similarity of these two quantities, despite their different microphysical origins, strongly hints at a common underlying mechanism linking baryogenesis and dark matter genesis. Within the SM, however, CP violation from the quark sector is insufficient by many orders of magnitude to account for the observed baryon asymmetry $\eta_B = 6.1 \times 10^{-10}$ [4], and no viable dark matter candidate exists. These facts motivate extensions of the SM that can simultaneously explain neutrino masses, CP violation, the baryon asymmetry of the Universe (BAU), and the relic abundance of dark matter—ideally from a single origin.

A particularly compelling approach to this problem is the asymmetric dark matter (ADM) hypothesis [7, 40], in which the relic density of dark matter arises from a particle–antiparticle asymmetry analogous to the baryon asymmetry in the visible sector. If both asymmetries originate from a common process that violates lepton or baryon number in the early Universe, their comparable abundances can be naturally explained. This idea is realized in baryon–dark matter co–genesis models [8, 10, 11], where visible and hidden asymmetries are generated simultaneously. Among the possible mechanisms, leptogenesis remains one of the most attractive, as it connects the cosmic matter asymmetry with the origin of neutrino masses [12, 13].

In standard thermal leptogenesis [13, 14], the CP–violating, out–of–equilibrium decays of heavy Majorana neutrinos create a lepton asymmetry that is partially converted to a baryon asymmetry through electroweak sphalerons. While this framework is elegant, it typically requires very heavy right–handed neutrinos ($M_N \gtrsim 10^{10}$ GeV) [12]. By contrast, in the resonant leptogenesis scenario [15, 16], a small mass splitting between nearly degenerate states can resonantly enhance the CP asymmetry, allowing successful baryogenesis even for masses in the range $M_N \sim 10^7$ – 10^9 GeV. In such cases, both the magnitude of the asymmetry and its flavor dependence are determined by the underlying Yukawa structure and CP phases.

The connection between leptogenesis and dark matter has been explored through several mechanisms in which the same heavy neutrino decays produce asymmetries in both the visible and hidden sectors [8, 10, 11]. Depending on the structure of the portal interactions, the resulting dark matter typically lies in the GeV range, yielding the correct ratio $\Omega_\chi/\Omega_B \sim 5$. Nevertheless, most existing constructions invoke multiple arbitrary couplings, additional mediator fields, or fine-tuned parameters. A symmetry–based explanation in

which the flavor structure, CP phases, and portal couplings all emerge from a common theoretical origin is still missing.

A natural step toward such a unified description arises from modular flavor symmetries [17, 18], a new paradigm that replaces the traditional flavon mechanism with modular forms. In this approach, Yukawa couplings are modular functions of a single complex modulus τ , which transforms under finite modular groups such as A_4 , S_4 , or A_5 . The vacuum expectation value (vev) of τ determines the entire flavor structure, while its complex phase provides an intrinsic source of CP violation. Modular invariant models have been shown to reproduce realistic neutrino mixing patterns consistent with NuFIT global data [19–21]. However, their implications for leptogenesis and asymmetric dark matter have remained largely unexplored.

In this work, we develop a modular S_4 –invariant framework that realizes resonant co–genesis of baryons and dark matter through a common source of CP violation determined by the modulus τ . The modular symmetry fixes all Yukawa couplings, linking the flavor structure of leptons directly to the parameters relevant for early–Universe asymmetry generation. The two quasi–degenerate fermionic triplets $\Sigma_{1,2}$ responsible for neutrino mass generation also drive the co–genesis process, establishing a direct connection between the neutrino and dark sectors.

Our construction employs the Type–III seesaw mechanism [22, 23], in which the heavy states are fermionic $SU(2)_L$ triplets with zero hypercharge. Unlike the singlet neutrinos of the Type–I seesaw, the triplet fields couple directly to the electroweak gauge bosons, providing richer phenomenology and potentially testable signatures at colliders. The effective light–neutrino mass matrix is generated through the relation

$$M_\nu \simeq -M_D^T M_\Sigma^{-1} M_D, \quad (1.2)$$

where M_D denotes the Dirac mass matrix and M_Σ the mass of the heavy triplets. The presence of $SU(2)_L$ interactions allows the triplet states to remain in equilibrium until temperatures close to their mass scale, ensuring the correct washout dynamics for resonant leptogenesis while naturally realizing a low seesaw scale ($M_\Sigma \sim 10^7$ GeV). Moreover, the same modular structure that fixes M_D also determines the couplings of Σ_i to the dark sector, thereby linking neutrino masses, leptonic CP violation, and dark matter co–genesis.

We solve the coupled Boltzmann equations describing the simultaneous evolution of lepton and dark asymmetries generated by Σ_1 decays [15, 16],

- $\Sigma_1 \rightarrow LH$ (lepton asymmetry $Y_{\Delta L}$) and $\Sigma_1 \rightarrow \chi\phi$ (dark asymmetry $Y_{\Delta\chi}$),
- including resonant CP violation, washout, and Σ –mediated transfer effects,
- with sphaleron conversion $Y_B = (28/79)Y_{\Delta L}$,
- yielding the DM relic ratio $\Omega_\chi/\Omega_B = (m_\chi/m_p)|Y_{\Delta\chi}/Y_{\Delta L}|$ [6].

All asymmetries are controlled by $\text{Re}(\tau)$, $\text{Im}(\tau)$ from the single modular parameter.

The remainder of this paper is organized as follows. Section 2 introduces the modular S_4 structure and the construction of the Yukawa couplings and the derivation of the neutrino mass matrices. Section 3 presents the Boltzmann framework describing co-genesis, while Section 4 contains the numerical analysis and benchmark predictions. Finally, Section 5 summarizes our conclusions and outlines possible phenomenological implications, including collider and gravitational-wave signatures.

2 Model

We consider a framework governed by the SM gauge symmetry $SU(2)_L \times U(1)_Y$, extended by a modular flavor symmetry S_4 of level 3 [17] and a discrete stabilizing symmetry Z_2^{DM} [6]. The modular symmetry governs the flavor structure of leptons, while Z_2^{DM} ensures the absolute stability of the dark matter candidate. In this construction, neutrino masses arise via a type-III seesaw mechanism [22, 23], and the baryon asymmetry is generated through leptogenesis [14]. A common fermion triplet mediator connects the visible and dark sectors, providing a unified origin for both the lepton asymmetry and the dark matter relic abundance [8].

The choice of the modular group S_4 is motivated by its ability to reproduce realistic lepton-mixing patterns through modular forms of low weight, avoiding the need for additional flavon fields [18]. Its vev $\langle \tau \rangle$ spontaneously breaks the modular invariance, fixing the modular forms $Y_i(\tau)$ that determine the Yukawa structures of both visible and dark sectors. For concreteness, τ is stabilized near the self-dual point $\tau = \omega = e^{2\pi i/3}$ [41], where the modular forms take fixed numerical values. The modular breaking scale $\Lambda_{\text{mod}} \sim 10^{10} \text{ GeV}$ lies above the seesaw mass scale $M_\Sigma \sim 10^7 \text{ GeV}$, thereby establishing a clear hierarchy between flavor generation and neutrino mass formation.

The field content and their transformation properties under $SU(2)_L \times U(1)_Y \times S_4 \times Z_2^{\text{DM}}$ are summarized in Table 1. The model introduces a fermionic $SU(2)_L$ triplet Σ , which plays a central role in neutrino mass generation and in mediating the visible–dark sector connection. The scalar doublets H_u and H_d are the Higgs fields responsible for electroweak symmetry breaking, while an additional scalar ϕ and a fermion χ constitute the dark sector. The fields ϕ and χ are odd under Z_2^{DM} , while all other fields remain even, preventing dark matter decay and ensuring the stability of χ [6].

The discrete parity Z_2^{DM} is assumed to be exact and unbroken by higher-dimensional or gravitational operators. Operators such as $(LH_u)\chi/\Lambda$ are forbidden since χ and ϕ are odd under Z_2^{DM} whereas all other fields are even. Loop-induced corrections respect this discrete symmetry, guaranteeing the stability of the dark fermion χ even in the presence of Planck-suppressed effects.

The modular forms appearing in the Yukawa interactions transform as multiplets of S_4 and are listed in Table 2. They carry modular weights corresponding to the order of the modular function, which determines the allowed couplings in the Lagrangian. The

Table 1. Transformation properties of matter and Higgs fields under $SU(2)_L \times U(1)_Y \times S_4 \times Z_2^{\text{DM}}$. The modular weights k_I are indicated in the last row.

Field	L	l_{R_1}	l_{R_2}	l_{R_3}	Σ	H_u	H_d	ϕ	χ
$SU(2)_L$	2	1	1	1	3	2	2	3	2
$U(1)_Y$	$-1/2$	-1	-1	-1	0	$+1/2$	$-1/2$	$+1/2$	$-1/2$
S_4	3	$1'$	1	$1'$	2	1	1	1	2
Z_2^{DM}	+	+	+	+	+	+	+	—	—
k_I	-2	0	-2	-2	-2	0	0	0	-2

Table 2. Transformation properties of modular Yukawa couplings under $SU(2)_L \times U(1)_Y \times S_4 \times Z_2^{\text{DM}}$. The modular weight k_I corresponds to the form weight.

	$Y_3^{(2)}$	$Y_{3'}^{(2)}$	$Y_1^{(4)}$	$Y_3^{(4)}$	$Y_{3'}^{(4)}$	$Y_2^{(4)}$
S_4	3	$3'$	1	3	$3'$	2
k_I	2	2	4	4	4	4

symmetry-breaking chain of the framework is expressed as

$$S_4^{\text{modular}} \times SU(2)_L \times U(1)_Y \xrightarrow[\langle \tau \rangle]{\text{spontaneous modular breaking}} SU(2)_L \times U(1)_Y \xrightarrow[\langle H_{u,d} \rangle = v]{\text{EWSB}} U(1)_{\text{em}}, \quad (2.1)$$

where $\langle \tau \rangle$ generates the modular forms that fix the Yukawa structures, while the Higgs vev $v \simeq 246$ GeV triggers electroweak symmetry breaking.

Each operator in the Lagrangian satisfies the modular weight conservation condition $\sum_i k_i + k_Y = 0$, ensuring modular invariance [17]. Explicitly,

$$\begin{aligned} (Ll_{R_1})_{\mathbf{3}'} H_d Y_{\mathbf{3}'}^{(2)} &: (-2) + (0) + (0) + (2) = 0, \\ (L\Sigma)_{\mathbf{3}} H_u Y_{\mathbf{3}}^{(4)} &: (-2) + (-2) + (0) + (4) = 0, \\ (\Sigma\chi\phi) Y_1^{(4)} &: (-2) + (-2) + (0) + (4) = 0. \end{aligned}$$

The complete Lagrangian of the model is written as

$$\mathcal{L} = \mathcal{L}_\ell + \mathcal{L}_D + \mathcal{L}_\Sigma + \mathcal{L}_{\text{DM}}, \quad (2.2)$$

where the terms correspond to the charged-lepton, Dirac-neutrino, Majorana, and dark-matter portal sectors, respectively.

The charged-lepton Yukawa couplings consistent with the modular S_4 symmetry take the form

$$\mathcal{L}_\ell = \alpha (Ll_{R_1})_{\mathbf{3}'} H_d Y_{\mathbf{3}'}^{(2)} + \beta (Ll_{R_2})_{\mathbf{3}} H_d Y_{\mathbf{3}}^{(4)} + \gamma (Ll_{R_3})_{\mathbf{3}'} H_d Y_{\mathbf{3}'}^{(4)} + \text{h.c.}, \quad (2.3)$$

which, after electroweak symmetry breaking, leads to the charged-lepton mass matrix

$$M_\ell = v_d \begin{pmatrix} \alpha Y_3 & -2\beta Y_2 Y_3 & 2\gamma Y_1 Y_3 \\ \alpha Y_5 & \beta(\sqrt{3} Y_1 Y_4 + Y_2 Y_5) & \gamma(\sqrt{3} Y_2 Y_4 - Y_1 Y_5) \\ \alpha Y_4 & \beta(\sqrt{3} Y_1 Y_5 + Y_2 Y_4) & \gamma(\sqrt{3} Y_2 Y_5 - Y_1 Y_4) \end{pmatrix}. \quad (2.4)$$

The Dirac neutrino mass term arises from

$$\mathcal{L}_D = \alpha_D (L\Sigma)_{\mathbf{3}} H_u Y_{\mathbf{3}}^{(4)} + \beta_D (L\Sigma)_{\mathbf{3}'} H_u Y_{\mathbf{3}'}^{(4)} + \text{h.c.}, \quad (2.5)$$

leading to the Dirac mass matrix M_D :

$$M_D = v_u \begin{pmatrix} -2\alpha_D Y_2 Y_3 & & -2\beta_D Y_1 Y_3 \\ -\alpha_D \left(\frac{\sqrt{3}}{2} Y_1 Y_4 + \frac{1}{2} Y_2 Y_5 \right) + \beta_D \left(\frac{3}{2} Y_2 Y_5 - \frac{\sqrt{3}}{2} Y_1 Y_4 \right) & \alpha_D \left(\frac{3}{2} Y_1 Y_5 + \frac{\sqrt{3}}{2} Y_2 Y_4 \right) + \beta_D \left(-\frac{3}{2} Y_1 Y_5 + \frac{\sqrt{3}}{2} Y_2 Y_4 \right) \\ -\alpha_D \left(\frac{\sqrt{3}}{2} Y_1 Y_5 + \frac{1}{2} Y_2 Y_4 \right) + \beta_D \left(\frac{3}{2} Y_2 Y_4 - \frac{\sqrt{3}}{2} Y_1 Y_5 \right) & \alpha_D \left(\frac{3}{2} Y_1 Y_4 + \frac{\sqrt{3}}{2} Y_2 Y_5 \right) + \beta_D \left(-\frac{3}{2} Y_1 Y_4 + \frac{\sqrt{3}}{2} Y_2 Y_5 \right) \end{pmatrix}. \quad (2.6)$$

The heavy Majorana mass term for Σ is given by

$$\mathcal{L}_\Sigma = \frac{1}{2} M Y_1^{(4)} \text{Tr}(\Sigma^c \Sigma) + \frac{1}{2} M_\epsilon \left(\Sigma^c \cdot Y_2^{(4)} \otimes \Sigma \right)_1 + \text{h.c.}, \quad (2.7)$$

yielding

$$M_\Sigma = \begin{pmatrix} M(Y_1^2 + Y_2^2) - M_\epsilon(Y_2^2 - Y_1^2) & M_\epsilon Y_1 Y_2 \\ M_\epsilon Y_1 Y_2 & M(Y_1^2 + Y_2^2) + M_\epsilon(Y_2^2 - Y_1^2) \end{pmatrix}. \quad (2.8)$$

The eigenvalues of M_Σ correspond to two quasi-degenerate heavy Majorana mass eigenstates $\Sigma_{1,2}$ with masses $M_{1,2}$, whose small modular-induced splitting enables resonant enhancement.

The light neutrino mass matrix is then obtained through the type-III seesaw relation,

$$M_\nu = -M_D M_\Sigma^{-1} M_D^T, \quad (2.9)$$

linking low-energy neutrino parameters directly to the modular structure.

Finally, the dark sector interacts through the portal coupling

$$\mathcal{L}_{\text{DM}} = y_{\text{DM}} \text{Tr}[\Sigma(\chi\phi)] Y_2^{(4)} + \text{h.c.}, \quad (2.10)$$

where χ is stabilized by the discrete symmetry \mathbb{Z}_2^{DM} , and y_{DM} denotes the dark-sector Yukawa coupling that controls the strength of the portal interaction between the heavy triplet Σ and the dark fields (χ, ϕ) . After the breaking of the modular S_4 symmetry, the modular form $Y_2^{(4)}(\tau)$ induces a specific flavor structure for the dark Yukawa coupling, which can be written as

$$Y_\chi = y_{\text{DM}} \begin{pmatrix} Y_1^2 - Y_2^2 & 2Y_1 Y_2 \\ 2Y_1 Y_2 & -Y_1^2 + Y_2^2 \end{pmatrix}. \quad (2.11)$$

This interaction transfers the generated lepton asymmetry to the dark sector through Σ exchange [8], resulting in correlated baryon and dark matter abundances. All coefficients $\alpha, \beta, \gamma, \alpha_D, \beta_D, M, M_\epsilon \sim \mathcal{O}(1)$ are real free parameters that can be traded for rescaled modular forms $Y_i \rightarrow \alpha_i Y_i(\tau = \omega)$, whose values are fixed by requiring realistic mass hierarchies consistent with oscillation data.

3 Leptogenesis and Asymmetric Dark Matter

In this section we describe a co-genesis scenario in which the BAU and the DM relic abundance originate simultaneously from the CP-violating decays of nearly degenerate heavy Majorana fermions [8, 9]. The framework relies on resonant leptogenesis [15] and incorporates a modular S_4 flavor structure, which ties the CP phases of the visible and dark sectors to a common complex modulus τ [17].

3.1 Co-genesis framework

The two heavy triplet states $\Sigma_{1,2}$ originate from the S_4 doublet Σ introduced in Sec. 2. A small mass splitting $\Delta M_\Sigma = |M_2 - M_1|$ is induced by the modular-symmetry-breaking parameter M_ϵ in Eq. (2.8), naturally realizing the quasi-degenerate spectrum required for resonant enhancement [15].

The relevant interactions governing leptogenesis and dark-matter asymmetry generation are

$$\mathcal{L} \supset -(Y_\nu)_{\alpha i} \overline{L_\alpha} \tilde{H}_u \Sigma_i - (Y_\chi)_i \overline{\chi} \phi \Sigma_i - \frac{1}{2} \overline{\Sigma_i^c} (M_\Sigma)_{ij} \Sigma_j + \text{h.c.}, \quad (3.1)$$

where $\tilde{H}_u = i\sigma_2 H_u^*$.

The modular forms determining these couplings follow from the assignments in Sec. 2:

$$Y_\nu \propto \alpha_D Y_{\mathbf{3}}^{(4)} + \beta_D Y_{\mathbf{3}'}^{(4)}, \quad Y_\chi \propto y_{DM} Y_{\mathbf{2}}^{(4)}, \quad M_\Sigma = M Y_{\mathbf{1}}^{(4)} + M_\epsilon Y_{\mathbf{2}}^{(4)}.$$

Hence the CP phases in both Y_ν and Y_χ originate from the same complex modulus τ .

The heavy fermions Σ_i decay through two competing channels,

$$\Sigma_i \rightarrow LH_u, \quad \Sigma_i \rightarrow \chi\phi, \quad (3.2)$$

producing CP asymmetries in both the visible and dark sectors. Since the dark scalar ϕ does not acquire a vev, it acts purely as a final-state field, ensuring the stability of the dark sector.

For the lighter state Σ_1 , the CP asymmetries are defined as

$$\epsilon_L = \frac{\Gamma(\Sigma_1 \rightarrow LH_u) - \Gamma(\Sigma_1 \rightarrow \bar{L}H_u^\dagger)}{\Gamma_{\Sigma_1}}, \quad \epsilon_\chi = \frac{\Gamma(\Sigma_1 \rightarrow \chi\phi) - \Gamma(\Sigma_1 \rightarrow \bar{\chi}\phi^\dagger)}{\Gamma_{\Sigma_1}}, \quad (3.3)$$

where Γ_{Σ_1} denotes the total decay width of Σ_1 .

3.2 Resonant CP asymmetries

In the resonant regime, the CP asymmetry is dominated by self-energy diagrams involving the nearly degenerate states Σ_i and Σ_j ($i \neq j$) see in Fig. 1 [15, 16, 24]. Neglecting vertex corrections and keeping only the resonantly enhanced self-energy piece, the CP asymmetries are

$$\epsilon_L^i = \frac{\text{Im} \left[(Y_\nu^\dagger Y_\nu)_{ij} \left((Y_\nu^\dagger Y_\nu + 2Y_\chi^\dagger Y_\chi)_{ij} \right) \right]}{8\pi (Y_\nu^\dagger Y_\nu + Y_\chi^\dagger Y_\chi)_{ii}} \frac{(M_i^2 - M_j^2) M_i \Gamma_j^{(0)}}{(M_i^2 - M_j^2)^2 + M_i^2 \Gamma_j^{(0)2}}, \quad (3.4)$$

$$\epsilon_\chi^i = \frac{\text{Im} \left[(Y_\chi^\dagger Y_\chi)_{ij} \left((2Y_\nu^\dagger Y_\nu + Y_\chi^\dagger Y_\chi)_{ij} \right) \right]}{8\pi (Y_\nu^\dagger Y_\nu + Y_\chi^\dagger Y_\chi)_{ii}} \frac{(M_i^2 - M_j^2) M_i \Gamma_j^{(0)}}{(M_i^2 - M_j^2)^2 + M_i^2 \Gamma_j^{(0)2}}, \quad (3.5)$$

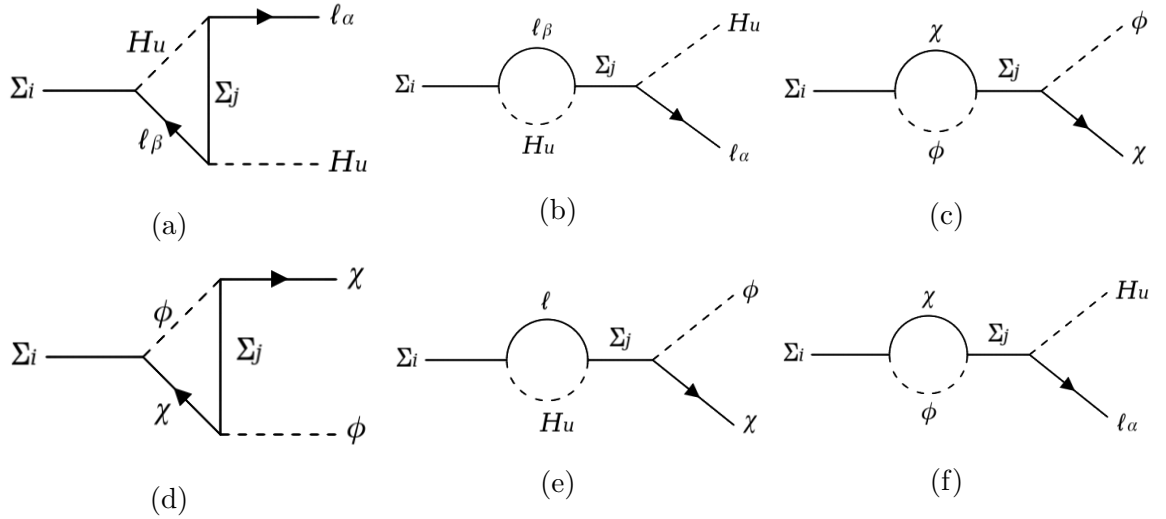


Figure 1. One-loop self-energy diagrams contributing to the CP asymmetries in the visible and dark sectors. The interference between tree-level and loop processes with intermediate triplet exchange induces unequal decay rates into $\ell_\alpha H$ and $\chi\phi$ versus their CP-conjugate channels.

where the tree-level width is

$$\Gamma_j^{(0)} \simeq \frac{M_j}{8\pi} [(Y_\nu^\dagger Y_\nu)_{jj} + (Y_\chi^\dagger Y_\chi)_{jj}],$$

including both CP-conjugate decay channels in the standard total-width normalization.

3.3 Decay widths and branching ratios

The total decay width of Σ_1 is

$$\Gamma_{\Sigma_1} = \Gamma(\Sigma_1 \rightarrow LH_u) + \Gamma(\Sigma_1 \rightarrow \chi\phi), \quad (3.6)$$

with partial widths

$$\Gamma(\Sigma_1 \rightarrow LH_u) = \frac{M_1^2}{8\pi v_u^2} \tilde{m}_1, \quad \Gamma(\Sigma_1 \rightarrow \chi\phi) = \frac{M_1^2}{8\pi v_u^2} \tilde{m}_{\text{dm}}, \quad (3.7)$$

which can be expressed in terms of the effective mass parameters

$$\tilde{m}_1 = \frac{|Y_\nu|^2 v_u^2}{M_1}, \quad \tilde{m}_{\text{dm}} = \frac{|Y_\chi|^2 v_u^2}{4M_1}. \quad (3.8)$$

The factor 1/4 in \tilde{m}_{dm} arises from the $SU(2)_L$ normalization of the triplet coupling. This normalization is consistently included in the total width appearing in the CP-asymmetry denominators.

The branching ratios into visible and dark sectors are therefore

$$\text{Br}_L = \frac{\Gamma(\Sigma_1 \rightarrow LH_u)}{\Gamma_{\Sigma_1}}, \quad \text{Br}_\chi = \frac{\Gamma(\Sigma_1 \rightarrow \chi\phi)}{\Gamma_{\Sigma_1}}, \quad (3.9)$$

where the dark Yukawa coupling contributes with an effective weight of 1/4 in the total width, as reflected in Br_χ through \tilde{m}_{dm} .

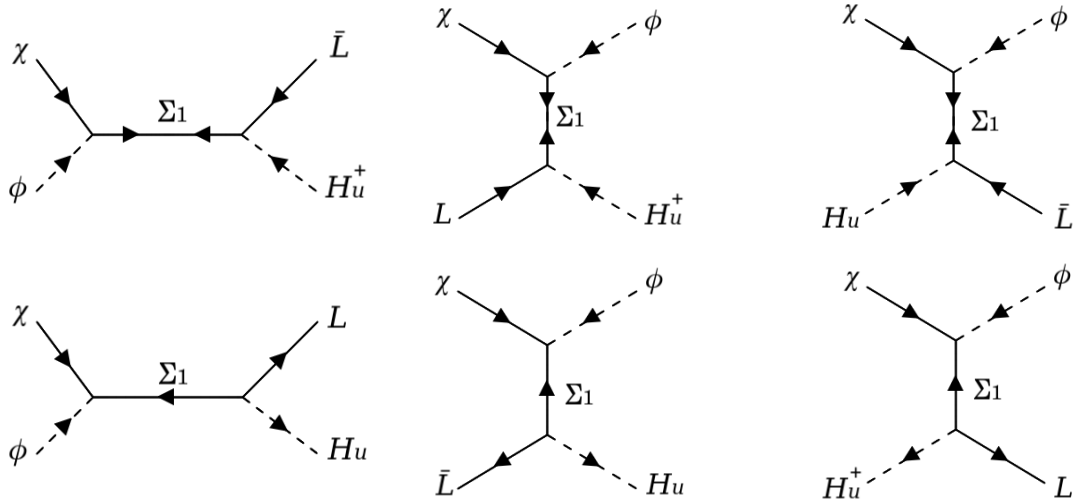


Figure 2. Feynman diagrams contributing to the $2 \rightarrow 2$ scattering processes entering the Boltzmann equations (3.11) and (3.12). The top row shows the $\Delta L = 2$ processes responsible for lepton-number-violating washout, while the bottom row displays the $\Delta L = 0$ transfer processes that mediate the exchange of the asymmetry between the visible and dark sectors.

3.4 Boltzmann evolution

Defining the washout parameter $K_1 \equiv \Gamma_{\Sigma_1}/H(z=1)$, the coupled Boltzmann equations [8] for the comoving abundances $Y_{\Sigma_1} = n_{\Sigma_1}/s$, $Y_{\Delta L} = Y_L - Y_{\bar{L}}$, and $Y_{\Delta\chi} = Y_\chi - Y_{\bar{\chi}}$ are

$$\frac{dY_{\Sigma_1}}{dz} = -\frac{\Gamma_1}{H(z=1)} z \frac{K_1(z)}{K_2(z)} (Y_{\Sigma_1} - Y_{\Sigma_1}^{\text{eq}}), \quad (3.10)$$

$$\begin{aligned} \frac{dY_{\Delta L}}{dz} = -\frac{\Gamma_1}{H(z=1)} & \left[\epsilon_L z \frac{K_1(z)}{K_2(z)} (Y_{\Sigma_1}^{\text{eq}} - Y_{\Sigma_1}) + 2\text{Br}_L^2 I_W(z) Y_{\Delta L} \right. \\ & \left. + \text{Br}_L \text{Br}_\chi \left(I_T^+(z) (Y_{\Delta L} + Y_{\Delta\chi}) + I_T^-(z) (Y_{\Delta L} - Y_{\Delta\chi}) \right) \right], \end{aligned} \quad (3.11)$$

$$\begin{aligned} \frac{dY_{\Delta\chi}}{dz} = -\frac{\Gamma_1}{H(z=1)} & \left[\epsilon_\chi z \frac{K_1(z)}{K_2(z)} (Y_{\Sigma_1}^{\text{eq}} - Y_{\Sigma_1}) + 2\text{Br}_\chi^2 I_W(z) Y_{\Delta\chi} \right. \\ & \left. + \text{Br}_L \text{Br}_\chi \left(I_T^+(z) (Y_{\Delta L} + Y_{\Delta\chi}) - I_T^-(z) (Y_{\Delta L} - Y_{\Delta\chi}) \right) \right], \end{aligned} \quad (3.12)$$

where $H(z)$ is the Hubble rate in the radiation-dominated era and $K_{1,2}(z)$ are modified Bessel functions. The functions $I_W(z)$ and $I_T^\pm(z)$ encode thermally averaged washout and transfer contributions from inverse decays and off-shell Σ_1 -mediated scatterings [8, 42], as detailed in Appendix C. These equations capture the interplay among decay, washout, and transfer processes that shape both asymmetries, as illustrated in Fig. 2.

3.5 Relic asymmetries and dark matter abundance

After Σ_1 decays freeze out, $Y_{\Delta L}$ and $Y_{\Delta\chi}$ become conserved. The lepton asymmetry is partially converted into a baryon asymmetry by electroweak sphalerons,

$$Y_B = c_{\text{sph}} Y_{\Delta L}, \quad c_{\text{sph}} = \frac{8}{23}, \quad (3.13)$$

which assumes Standard Model field content and efficient sphaleron conversion above the electroweak scale [13]. The symmetric component of χ annihilates efficiently through t -channel ϕ exchange since $m_\chi \simeq 0.1\text{--}2\text{ GeV} \ll m_\phi \simeq 100\text{ GeV}$, rendering $\chi\bar{\chi} \rightarrow \phi\phi$ kinematically forbidden, leaving only the asymmetric relic contribution relevant at late times. The present-day energy-density ratio of dark matter to baryons is

$$\frac{\Omega_\chi}{\Omega_B} = \frac{m_\chi}{m_p} \frac{|Y_{\Delta\chi}|}{|Y_{\Delta L}|}, \quad (3.14)$$

where m_p is the proton mass. The observed ratio $\Omega_\chi/\Omega_B \simeq 5.4$ [4] implies that comparable visible and dark asymmetries naturally correspond to $m_\chi \simeq 0.1\text{--}2\text{ GeV}$.

Once Σ_1 has decayed completely, the asymmetries saturate to constant values $Y_{\Delta L}^\infty$ and $Y_{\Delta\chi}^\infty$, leading to [40]

$$\Omega_\chi h^2 = \frac{m_\chi s_0 |Y_{\Delta\chi}^\infty|}{\rho_c/h^2}, \quad \rho_c/h^2 = 1.05 \times 10^{-5} \text{ GeV cm}^{-3}, \quad (3.15)$$

and therefore

$$m_\chi \simeq m_p \frac{\Omega_\chi}{\Omega_B} \left| \frac{Y_{\Delta L}^\infty}{Y_{\Delta\chi}^\infty} \right| \simeq 5.4 m_p \left| \frac{Y_{\Delta L}^\infty}{Y_{\Delta\chi}^\infty} \right|. \quad (3.16)$$

If $\text{Br}_\chi > \text{Br}_L$, the dark asymmetry is larger and Eq. (3.16) predicts a correspondingly heavier ADM candidate, linking the DM and neutrino mass scales through the same modular origin of CP violation.

Overall, this framework quantitatively connects neutrino masses, baryon asymmetry, and dark matter abundance, all governed by the common modular parameter τ that controls both flavor and CP violation.

4 Numerical Analysis

4.1 Neutrino Sector

Table 3. NuFIT 5.2 (2024) best-fit values and 3σ ranges for normal hierarchy.

Parameter	Best-fit $\pm 1\sigma$	3σ range
$\sin^2 \theta_{12}$	$0.307^{+0.012}_{-0.011}$	$0.275 - 0.345$
$\sin^2 \theta_{23}$	$0.561^{+0.012}_{-0.015}$	$0.430 - 0.596$
$\sin^2 \theta_{13}$	$0.02195^{+0.00054}_{-0.00058}$	$0.02023 - 0.02376$
Δm_{21}^2 [10 $^{-5}$ eV 2]	$7.49^{+0.19}_{-0.19}$	$6.92 - 8.05$
Δm_{31}^2 [10 $^{-3}$ eV 2]	$2.534^{+0.025}_{-0.023}$	$2.463 - 2.606$

The numerical analysis has been performed for the normal hierarchy of neutrino masses within the modular S_4 framework. The light-neutrino mass matrix is obtained from the type-III seesaw relation $M_\nu = -M_D M_\Sigma^{-1} M_D^T$ [22, 23], where all entries of M_D and M_Σ are determined by the modular forms $Y_i(\tau)$ defined in Appendix A. The physical lepton

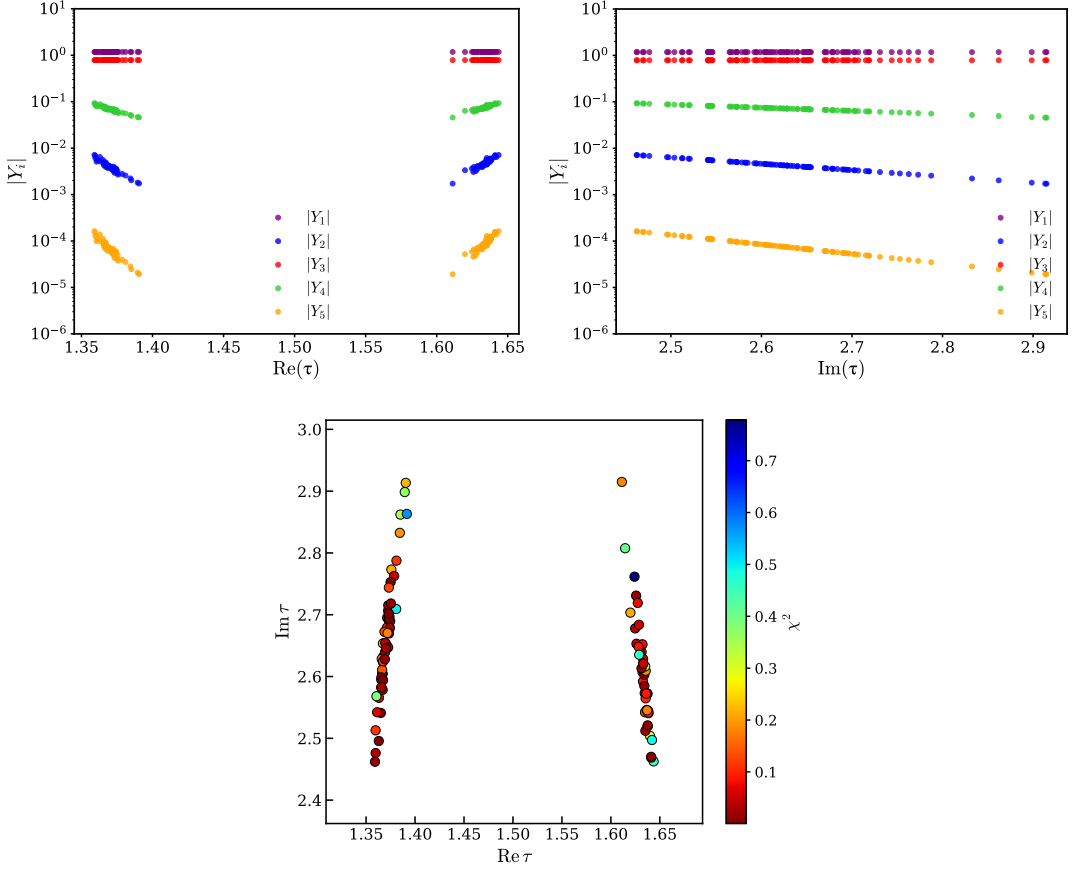


Figure 3. Allowed region of the complex modulus τ in the modular S_4 framework. Upper: absolute values of modular Yukawa forms $|Y_i|$ versus $\text{Re } \tau$ (left) and $\text{Im } \tau$ (right). Lower: χ^2 distribution in the $(\text{Re } \tau, \text{Im } \tau)$ plane. All displayed points lie within the NuFIT 5.2 3σ ranges.

mixing matrix is constructed as $U_{\text{PMNS}} = U_\ell^\dagger U_\nu$ [26], with U_ℓ and U_ν diagonalizing $M_\ell M_\ell^\dagger$ and M_ν , respectively. All oscillation observables are computed in the standard PMNS parametrization,¹ and the resulting predictions are compared with the NuFIT 5.2 (2024) global analysis for normal ordering [27]. The corresponding 3σ ranges are summarized in Table 3.

The input parameters are varied within the domains

$$\begin{aligned}
 1.0 < \text{Re } \tau < 2.0, & \quad 0.5 < \text{Im } \tau < 3.0, & \quad 0.5 < \alpha < 1.6, \\
 0.3 < \beta < 1.1, & \quad 1.0 < \gamma < 1.6, & \quad 10^{-3} < \alpha_D < 10^{-2}, \\
 10^{-5} < \beta_D < 10^{-3}, & \quad 5 \times 10^2 \text{ GeV} < M < 5 \times 10^3 \text{ GeV}, & \quad 10^5 \text{ GeV} < M_\epsilon < 5 \times 10^7 \text{ GeV}.
 \end{aligned}$$

For each parameter set, the modular Yukawa couplings are determined by the chosen τ , thereby fixing the flavor structure entirely through the S_4 modular forms [17]. The resulting parameter space is constrained by the NuFIT 5.2 3σ limits on mixing angles and mass-squared differences [27], as well as the Planck bound $\sum m_\nu < 0.12 \text{ eV}$ [4].

¹Explicit definitions of $\sin^2 \theta_{ij}$, δ_{CP} , and $m_{\beta\beta}$ are given in Appendix B.

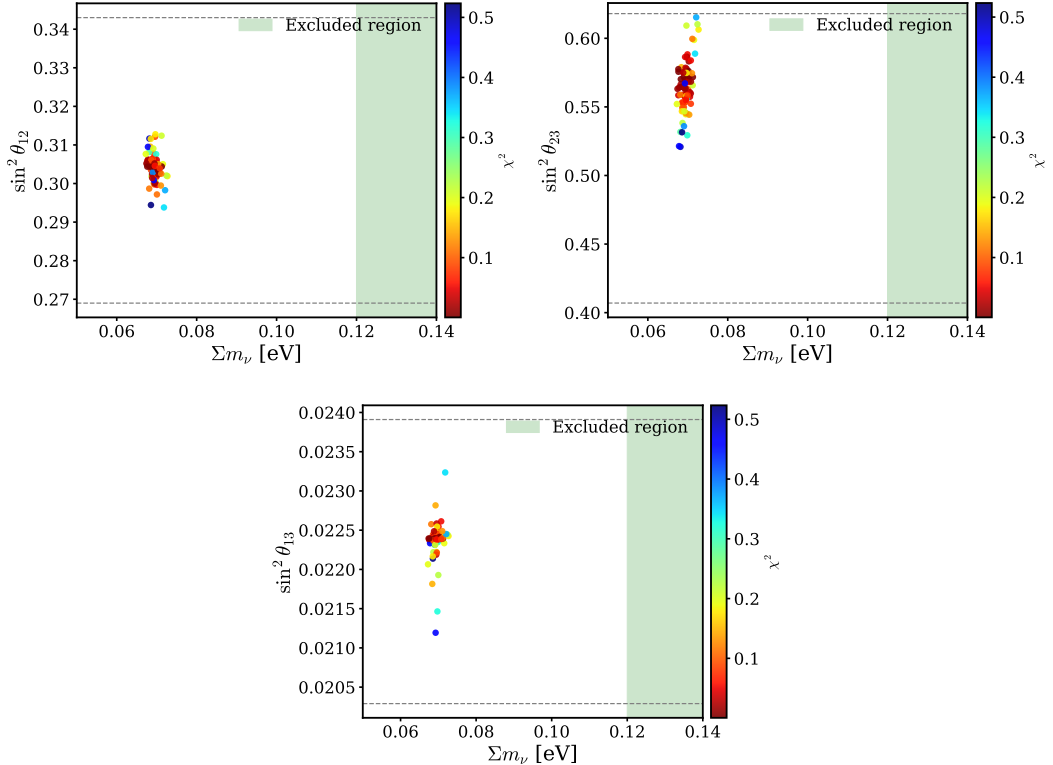


Figure 4. Correlations between the total neutrino mass $\sum m_\nu$ and the mixing angles $\sin^2 \theta_{12}$ (upper left), $\sin^2 \theta_{23}$ (upper right), and $\sin^2 \theta_{13}$ (lower panel). Dashed lines denote the 3σ ranges from NuFIT 5.2, and the shaded band shows the cosmological bound $\sum m_\nu < 0.12$ eV.

The region of the complex modulus τ consistent with neutrino oscillation data is displayed in Fig. 3, showing that acceptable solutions cluster around two narrow bands near $\text{Re } \tau \simeq 1.35$ and $\text{Re } \tau \simeq 1.63$ with $\text{Im } \tau \simeq 2.6\text{--}2.8$. These regions correspond to points where the modular Yukawa structures reproduce all neutrino mixing angles and mass-squared differences within the 3σ NuFIT 5.2 ranges, thereby phenomenologically fixing the modulus. In this framework, τ is not stabilized by an explicit potential but is effectively determined by requiring simultaneous agreement with low-energy neutrino observables, a standard approach in modular-flavor analyses [32, 43]. The localization of τ close to the self-dual point $\omega = e^{2\pi i/3}$ reflects the geometric properties of modular forms, which naturally yield hierarchical and stable Yukawa textures in this region. The magnitudes of the modular couplings exhibit the ordering $|Y_1| \gg |Y_3| > |Y_2| > |Y_4| > |Y_5|$ as shown in upper panel of Fig. 3, consistent with realistic lepton mass hierarchies. The apparent flatness of the modular Yukawas arises from the exponential suppression of higher-order q -terms ($q = e^{2\pi i\tau}$) for large $\text{Im } \tau$, leading to quasi-degenerate modular textures in a phenomenologically preferred τ region that simultaneously accounts for flavor and CP observables.

The correlations between $\sum m_\nu$ and the mixing angles are shown in Fig. 4. All viable points lie below the cosmological limit $\sum m_\nu < 0.12$ eV and fall within the 3σ regions of the global fit. The results indicate $\sum m_\nu \simeq (0.06\text{--}0.08)$ eV, $\sin^2 \theta_{12} \simeq 0.30$, $\sin^2 \theta_{23} \simeq 0.57$,

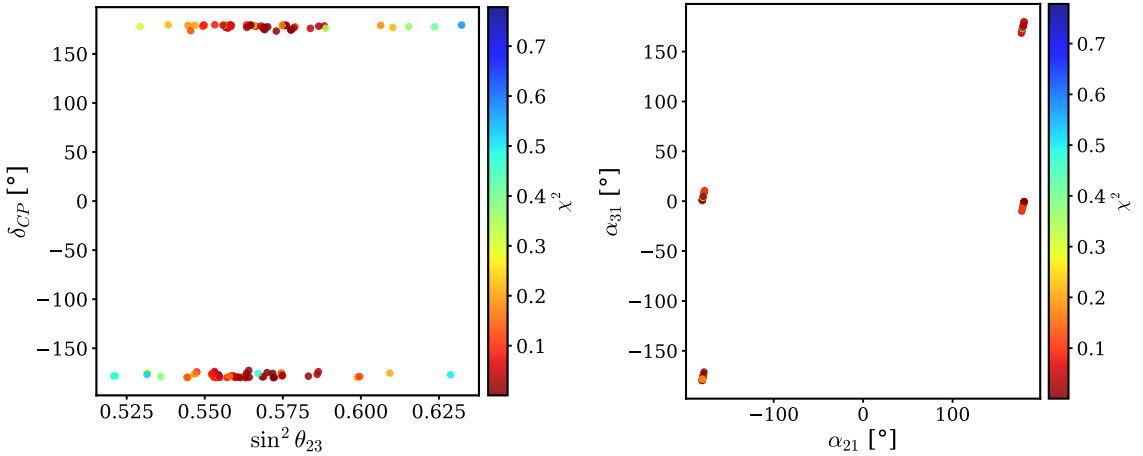


Figure 5. Left: correlation between δ_{CP} and $\sin^2 \theta_{23}$, showing near-maximal CP violation. Right: predicted Majorana phase structure $(\alpha_{21}, \alpha_{31})$ exhibiting discrete clustering near $(0, \pi)$ and $(\pm\pi/2, \pm\pi/2)$, a distinctive imprint of the modular symmetry.

and $\sin^2 \theta_{13} \simeq 0.022$, providing an excellent match to data and confirming that the model favors the normal ordering.

The atmospheric mixing angle and CP phase satisfy $\sin^2 \theta_{23} \simeq 0.56\text{--}0.59$ and $\delta_{CP} \in [\pm 150^\circ, \pm 180^\circ]$, as displayed in Fig. 5, implying nearly maximal CP violation. The predicted Majorana phases cluster around $(0, \pi)$ and $(\pm\pi/2, \pm\pi/2)$, reflecting the discrete modular structure of the Yukawa sector.

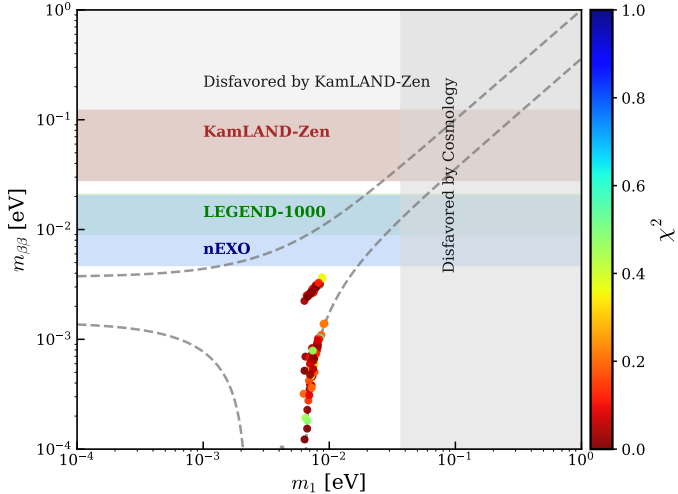


Figure 6. Effective Majorana mass $m_{\beta\beta}$ versus the lightest neutrino mass m_1 . Colored bands denote the current and projected sensitivities of KamLAND-Zen, LEGEND-1000, and nEXO.

The effective Majorana mass relevant for neutrinoless double beta decay, $m_{\beta\beta} = |m_1 U_{e1}^2 + m_2 U_{e2}^2 + m_3 U_{e3}^2|$ [28], is found to be in the range $m_{\beta\beta} \simeq (8\text{--}18) \times 10^{-3}$ eV, as shown in Fig. 6. This lies below the current KamLAND-Zen bound [29] but within the

future reach of nEXO [31] and LEGEND-1000 [30].

The modular S_4 framework with type-III seesaw successfully reproduces all neutrino oscillation observables within 3σ without fine-tuning, with the entire flavor structure governed by a single modulus τ . Since the same Yukawa couplings (Y_ν) and triplet masses (M_1, M_2) also control the decay asymmetries of the heavy fermions, these neutrino-determined parameters directly constrain the CP-violating sources for leptogenesis. The next section explores how this common structure naturally links baryon asymmetry and dark matter relic abundance through resonant co-genesis.

4.2 Baryon–Dark Matter Co-genesis

Having established the theoretical setup in Section 3, we now present a detailed numerical study of the correlated generation of the baryon asymmetry and ADM within the neutrino-viable modular S_4 framework. All Yukawa couplings, CP phases, and decay parameters entering leptogenesis are derived from the modular forms $Y_i(\tau)$ fixed by the same complex modulus τ that governs the neutrino sector. Hence, no additional free phases are introduced for baryogenesis or ADM production [32].

The CP asymmetries ϵ_L and ϵ_χ are evaluated using the modular Yukawa structures defined in Eqs. (3.4)–(3.5), within the neutrino-consistent parameter space obtained in Section 4. The phenomenologically relevant region of the complex modulus τ is restricted to two narrow bands centered at $\text{Re } \tau \simeq 1.37$ and 1.64 with $\text{Im } \tau \simeq 2.6\text{--}2.8$, where the modular forms develop sizable imaginary components. For each allowed τ , the corresponding Yukawa matrices (Y_ν, Y_χ) are constructed and inserted into the loop-induced decay asymmetry expressions, yielding the visible and dark sector CP parameters ϵ_L and ϵ_χ . The relative magnitudes of ϵ_L and ϵ_χ are further controlled by the portal coupling y_{DM} appearing in Eqs. (2.10). Although the modular structure fixes the relative phases of the two sectors, the value of y_{DM} determines their relative decay branching fractions and hence the dominant source of CP violation. For $y_{\text{DM}} \lesssim 10^{-3}$, the dark decay $\Sigma_1 \rightarrow \chi \phi$ dominates, yielding a larger dark asymmetry. At $y_{\text{DM}} \sim 10^{-2}$, the visible and dark CP asymmetries become nearly identical, $|\epsilon_L| \simeq |\epsilon_\chi|$, reflecting their common modular origin. This regime corresponds to balanced co-genesis, where both sectors freeze out with comparable asymmetries. A representative illustration of the y_{DM} dependence of the CP asymmetry ratio is provided in Appendix D, confirming the robustness of our numerical results.

The resulting distributions of $|\epsilon_L|$ and $|\epsilon_\chi|$ as functions of the heavy-triplet mass M_1 are shown in Fig. 7, while the variation of $|\epsilon_L|$ in the complex τ plane is displayed in Fig. 8. Both quantities lie in the range $10^{-9}\text{--}10^{-6}$ throughout the neutrino-viable parameter space, sufficient to account for the observed baryon asymmetry after including washout effects. The mild spread visible in Fig. 7 thus reflects not only the small modular-phase differences but also the variation in y_{DM} that controls the visible–dark balance.

The resonant enhancement characteristic of this regime amplifies the CP violation by a factor of $\mathcal{O}(10^{2\text{--}3})$, compensating for the relatively small Yukawa couplings $|Y_{\nu,\chi}| \sim 10^{-3}$ without the need for any fine-tuning. Although both ϵ_L and ϵ_χ are governed by the same complex modulus τ , they are not exactly proportional. The visible-sector Yukawa matrix $Y_\nu \sim (Y_{\mathbf{3}}^{(4)}, Y_{\mathbf{3}'}^{(4)})$ and the dark-sector coupling $Y_\chi \sim Y_{\mathbf{2}}^{(4)}$ transform under different S_4

multiplets and carry distinct modular weights. As a result, their complex phases are correlated but not identical, leading to comparable—though not perfectly matched—CP asymmetries in the two sectors. This feature is evident in Figs. 7(a,b), where both $|\epsilon_L|$ and $|\epsilon_\chi|$ cluster around the same order of magnitude but exhibit visible scatter. The heatmap in Fig. 8 further highlights that the maximal CP violation occurs precisely within the neutrino-viable τ bands, confirming that, in this framework, the imaginary part of τ acts as the sole physical source of CP violation.

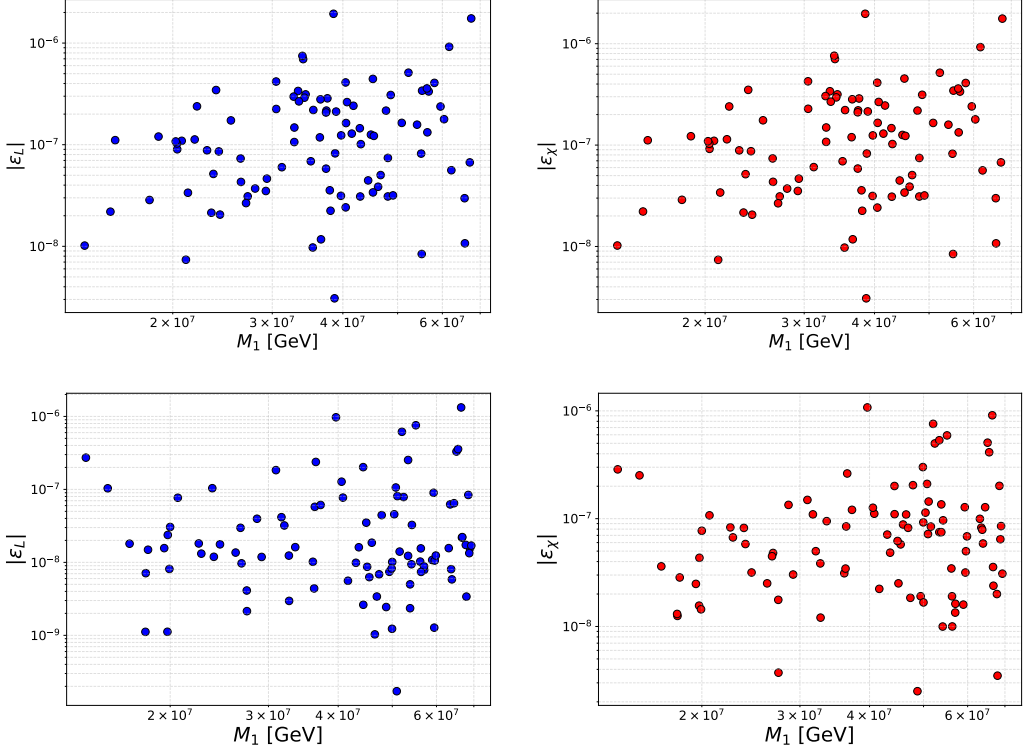


Figure 7. CP asymmetries as functions of the lightest heavy-triplet mass M_1 for two representative values of the dark-sector Yukawa coupling y_{DM} . Upper panels: $y_{\text{DM}} = 10^{-2}$ (balanced co-genesis regime with $|\epsilon_L| \simeq |\epsilon_\chi|$); lower panels: $y_{\text{DM}} = 10^{-3}$ (dark-dominated regime with $|\epsilon_\chi| > |\epsilon_L|$). Left: visible-sector asymmetry $|\epsilon_L|$; right: dark-sector asymmetry $|\epsilon_\chi|$.

To illustrate the quantitative realization of perfect co-genesis, we select benchmark points (BP1–BP4) from the neutrino-oscillation consistent τ region, each reproducing the observed baryon asymmetry and dark matter relic density within the 3σ NuFIT 5.2 limits. The corresponding parameters and cosmological observables are summarized in Table 4. These benchmarks serve as representative examples for the subsequent Boltzmann evolution.

The left panel presents the thermally averaged decay, washout, and transfer rates normalized to the Hubble expansion. At early times ($z = M_1/T < 1$) the total decay rate Γ_D/H is several orders of magnitude above unity, keeping Σ_1 in thermal equilibrium. As the Universe cools and z approaches unity, the decay rate falls below the Hubble expansion,

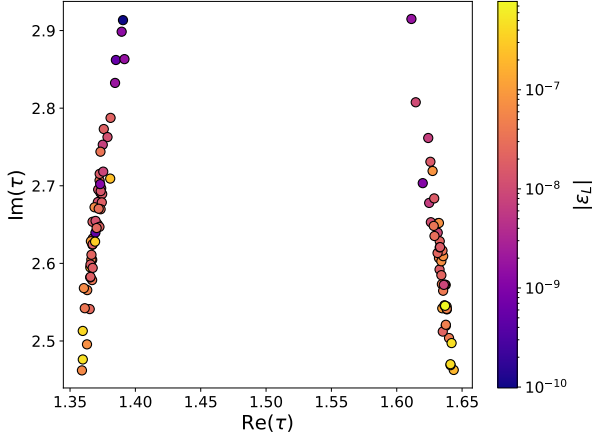


Figure 8. Magnitude of the CP asymmetry $|\epsilon_L|$ in the complex τ plane. The two allowed τ bands around $\text{Re} \tau \simeq 1.37$ and 1.64 with $\text{Im} \tau \simeq 2.6$ – 2.8 coincide with the neutrino-viable region, confirming that the imaginary part of τ acts as the sole physical source of CP violation.

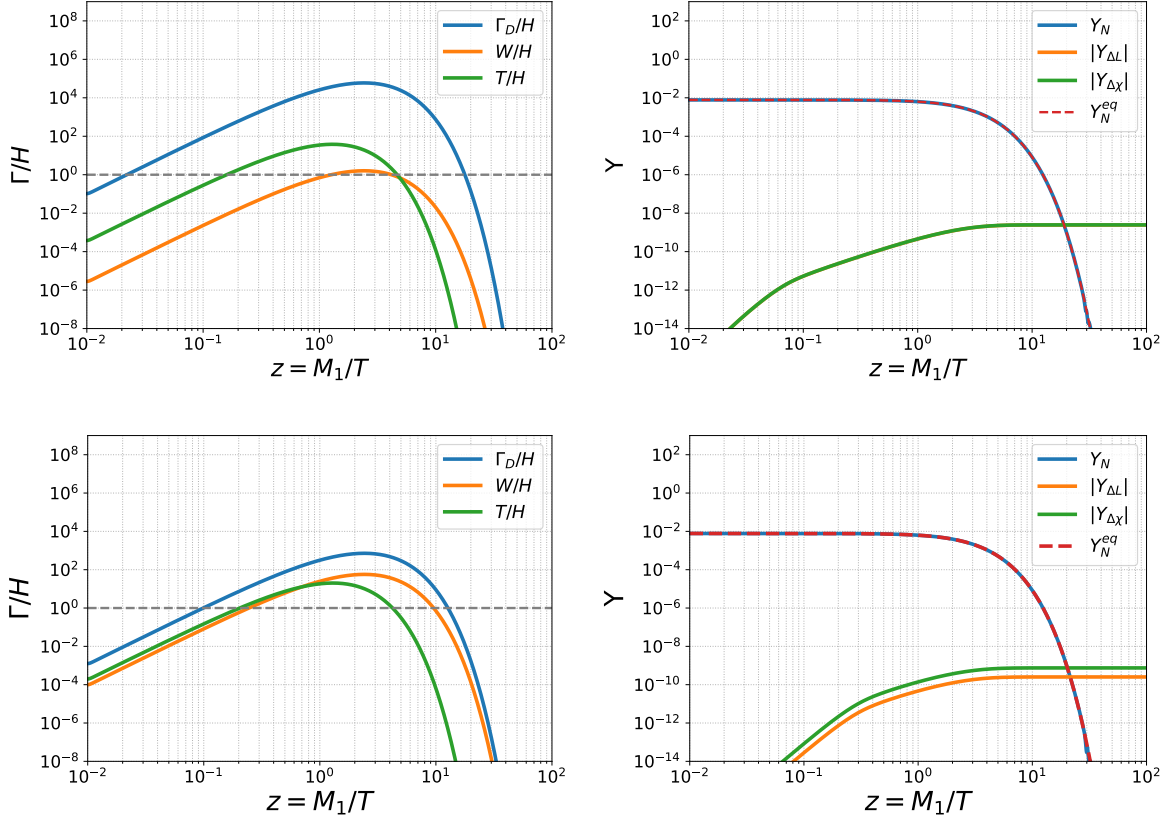


Figure 9. Boltzmann evolution for benchmark points BP4 (**upper row**, $y_{\text{DM}} = 10^{-2}$, balanced cogenesis) and BP1 (**lower row**, $y_{\text{DM}} = 10^{-3}$, dark-dominated). Left: thermally averaged decay, washout, and transfer rates as functions of $z = M_1/T$. Right: comoving yields of the heavy triplet and the lepton and dark asymmetries. Both asymmetries freeze out around $z \gtrsim 6$, with co-genesis realized near intermediate y_{DM} values.

Table 4. Benchmark points illustrating the transition between dark- and balanced co-genesis regimes. All benchmarks reproduce the observed baryon asymmetry and dark relic density within uncertainties.

Point	τ	M_1 [10 ⁷ GeV]	$ \epsilon_L $	$ \epsilon_\chi $	η_B	$\Omega_\chi h^2$	Ω_χ/Ω_B	m_χ [GeV]
$y_{\text{DM}} = 10^{-3}$ (dark-dominated)								
BP1	$1.37 + i2.63$	1.9	2.3×10^{-8}	4.3×10^{-7}	4.6×10^{-10}	0.10	4.03	0.97
BP2	$1.64 + i2.57$	2.1	3.05×10^{-8}	7.72×10^{-8}	5.9×10^{-10}	0.116	5.19	0.70
$y_{\text{DM}} = 10^{-2}$ (balanced co-genesis)								
BP3	$1.64 + i2.52$	1.96	3.17×10^{-8}	3.19×10^{-8}	6.15×10^{-10}	0.121	5.4	1.78
BP4	$1.37 + i2.69$	4.16	3.37×10^{-8}	3.39×10^{-8}	6.5×10^{-10}	0.12	5.7	1.76

marking the onset of the out-of-equilibrium regime required by the Sakharov conditions. The washout (W/H) and transfer (T/H) processes remain much smaller than unity during this epoch, ensuring that the generated asymmetries are only mildly erased.

The Boltzmann evolution of the heavy triplet and the resulting asymmetries is shown in Fig. 9 (right panel) for representative portal couplings $y_{\text{DM}} = 10^{-3}$ and 10^{-2} , corresponding respectively to benchmark points BP1 (dark-dominated) and BP3 (balanced co-genesis) listed in Table 4. In both cases, the triplet remains in thermal equilibrium for $z < 1$ and departs near $z \simeq 1$, satisfying the out-of-equilibrium condition required for leptogenesis. Once the decays of Σ_1 become inefficient ($z \gtrsim 1$), CP-violating decays generate simultaneous lepton and dark asymmetries. The comoving yields Y_N , $|Y_{\Delta L}|$, and $|Y_{\Delta \chi}|$ evolve as shown in the right panels of Fig. 9: both asymmetries grow and freeze out around $z \gtrsim 6$, when $\Gamma_D/H \ll 1$. For small y_{DM} , the dark yield $|Y_{\Delta \chi}|$ dominates, while at larger y_{DM} the visible and dark yields become comparable, reflecting their nearly equal CP asymmetries. The balanced co-genesis regime is therefore realized around $y_{\text{DM}} \sim 10^{-2}$, where $|Y_{\Delta L}^\infty| \simeq |Y_{\Delta \chi}^\infty|$. Other benchmark points exhibit qualitatively similar evolution with only mild variations in the final asymmetry ratios, so BP1 and BP3 sufficiently illustrate the generic behavior of the co-genesis dynamics in this framework.

4.3 Correlation between CP Asymmetries and Relic Densities

The solutions of the coupled Boltzmann equations (3.10)–(3.12) for the benchmark points in Table 4 yield the final asymmetries $Y_{\Delta L}^\infty$ and $Y_{\Delta \chi}^\infty$, which are subsequently converted into the baryon and dark matter relic abundances through Eqs. (3.13)–(3.15) [33]. Fig. 10 illustrates the numerical correlation between microscopic CP asymmetries ($\epsilon_L, \epsilon_\chi$) and macroscopic observables η_B and $\Omega_\chi h^2$. Both balanced co-genesis and dark-sector dominated regimes are included in this combined τ -scan. Their contributions appear as a mild spread in the correlation plots, reflecting the small variations of the branching ratios and CP phases across the parameter space.

At fixed heavy-triplet mass M_1 , both η_B and $\Omega_\chi h^2$ scale linearly with the corresponding CP asymmetries for small $|\epsilon_{L,\chi}|$, as expected when washout is not yet saturated. Beyond this range, partial washout effects flatten the growth of the generated asymmetries, reflecting the onset of asymmetry damping. Across the neutrino-viable τ region, the baryon asymmetry consistently falls near the observed value $\eta_B^{\text{obs}} = (6.12 \pm 0.03) \times 10^{-10}$ [4], while

the dark relic density matches the Planck constraint $\Omega_\chi h^2 = 0.12 \pm 0.001$, demonstrating that both sectors reach the correct magnitudes without additional parameter tuning. Because ϵ_χ tracks ϵ_L up to $\mathcal{O}(1)$ factors, the linear trend with $|\epsilon_L|$ in Fig. 10(a) effectively captures the behavior of both CP sources.

Numerically, the ratio Ω_χ/Ω_B stabilizes in a narrow band $\Omega_\chi/\Omega_B \simeq 5\text{--}7$, fully consistent with the cosmological value $\Omega_\chi/\Omega_B \simeq 5.4$. The mild spread arises from small $\mathcal{O}(1)$ differences between the modular phases of Y_ν and Y_χ , confirming that the co-genesis correlation originates directly from the modular flavor geometry rather than from any ad-hoc phase tuning.

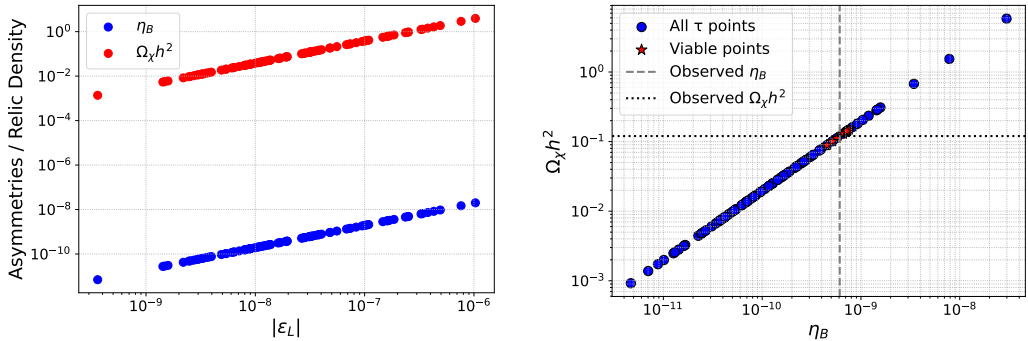


Figure 10. Correlation between microscopic CP asymmetries and macroscopic relic observables. (a) Baryon asymmetry η_B (blue) and dark matter relic density $\Omega_\chi h^2$ (red) as functions of the CP asymmetry $|\epsilon_L|$, showing linear scaling in the regime of unsaturated washout and mild saturation at larger values. (b) Direct correlation between $\Omega_\chi h^2$ and η_B for all τ points (blue) and neutrino-viable points (red stars), demonstrating co-genesis near the observed values $\eta_B^{\text{obs}} = 6.12 \times 10^{-10}$ and $\Omega_\chi h^2 = 0.12$.

Overall, the modular S_4 structure enforces a robust correlation at the order-of-magnitude level between ϵ_L , ϵ_χ , and the final relic abundances. Since the same modulus τ governs both visible and dark CP violation, the observed Ω_χ/Ω_B ratio emerges naturally from the modular geometry, providing a unified and predictive framework for baryon–dark matter co-genesis. Because ϵ_χ tracks ϵ_L up to $\mathcal{O}(1)$ factors, the linear trend with $|\epsilon_L|$ in Fig. 10 effectively captures the behavior of both CP sources. For clarity, we present the correlation using the dark-sector asymmetry $|\epsilon_\chi|$ follows the same trend due to their common modular origin and comparable magnitudes across the viable parameter space.

4.4 Dependence on Dark Matter Mass and Benchmark Predictions

To further quantify the co-genesis mechanism, we analyze the dependence of the dark matter relic density $\Omega_\chi h^2$ and the ratio Ω_χ/Ω_B on the dark fermion mass m_χ . The results are obtained by solving the Boltzmann equations for the benchmark points in Table 4, keeping all other parameters fixed to their neutrino-viable modular values.

Figure 11 shows that both quantities scale approximately linearly with m_χ once the dark and visible asymmetries $Y_{\Delta\chi}^\infty$ and $Y_{\Delta L}^\infty$ have frozen out. In this regime, the relic abundance follows $\Omega_\chi h^2 \propto m_\chi |Y_{\Delta\chi}^\infty|$, and the ratio Ω_χ/Ω_B increases proportionally with

m_χ . All benchmark trajectories nearly coincide, indicating that the freeze-out asymmetries are very similar throughout the neutrino-consistent τ region. The intersection with the observed Planck values, $\Omega_\chi h^2 = 0.120 \pm 0.001$ and $\Omega_\chi/\Omega_B \simeq 5.4$ [4], occurs for

$$m_\chi \simeq (0.1\text{--}2) \text{ GeV}, \quad (4.1)$$

in excellent agreement with the numerical benchmarks in Table 4.

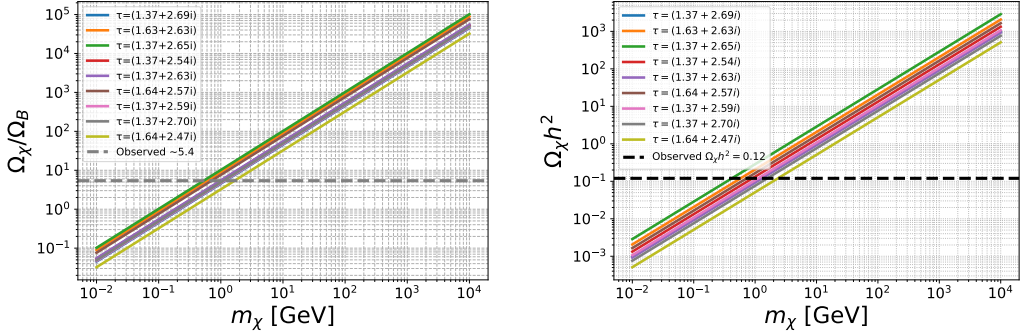


Figure 11. Dependence of the relic abundances on the dark matter mass m_χ for the benchmark points in Table 4. Left: ratio Ω_χ/Ω_B as a function of m_χ . Right: dark matter relic density $\Omega_\chi h^2$ versus m_χ . Both show an approximately linear trend once the asymmetry is frozen, and all benchmark trajectories nearly coincide, reflecting the small spread of freeze-out asymmetries across the viable τ region.

Because the same τ -controlled CP asymmetries determine both $Y_{\Delta L}^\infty$ and $Y_{\Delta \chi}^\infty$, the preferred value $m_\chi \simeq 0.5\text{--}2 GeV effectively encodes neutrino-sector information in the dark matter mass prediction. The resulting m_χ is therefore not imposed by hand, but emerges naturally from the modular S_4 dynamics that govern both visible and dark asymmetry generation.$

Remarks on theoretical assumptions. The present analysis is based on the supersymmetric modular S_4 framework, so it is worth clarifying how the different energy scales remain consistent within the framework. The model is analyzed in the effective non-supersymmetric limit, yet it can naturally arise from a supersymmetric or supergravity completion in which the modulus τ and its associated modular functions $Y_i(\tau)$ originate from a chiral modulus field. Supersymmetry breaking may be represented by a spurion field $X = \theta^2 F$, which transmits soft terms of typical size $m_{\text{SUSY}} \simeq F/M_{\text{mess}}$, where M_{mess} is the mediation scale[17].

In the parameter range explored here, the heavy fermionic triplets have characteristic masses

$$M_\Sigma \sim 10^7 \text{ GeV},$$

while the dark matter mass remains in the few-GeV regime. A plausible and phenomenologically stable hierarchy of

$$m_{\text{SUSY}} \sim 10^{6\text{--}8} \text{ GeV}, \quad M_{\text{mess}} \sim 10^{14\text{--}16} \text{ GeV},$$

leads to a ratio $m_{\text{SUSY}}/M_{\text{mess}} \lesssim 10^{-8}$, which keeps any supersymmetric threshold effects on the modular Yukawa structure extremely small.

Because of this suppression, the modular flavor relations remain radiatively stable, and the predictions derived from them are not distorted by higher-scale corrections. Furthermore, all possible superpartners are expected to decouple well before the leptogenesis epoch, leaving a consistent low-energy theory that contains only the Standard Model fields, the fermionic triplets Σ_i , and the dark-sector fields (χ, ϕ) . This ensures that the effective description used in our analysis remains valid throughout the relevant cosmological evolution.

Time dependence of the CP asymmetry. In resonant leptogenesis, a full quantum treatment reveals that the CP asymmetry $\epsilon(t)$ can exhibit oscillatory time dependence when the mass splitting ΔM becomes comparable to the decay width Γ [34]. In the present analysis, we employ the standard momentum-averaged Boltzmann formalism [35], using time-independent asymmetries $\epsilon_{L,\chi}$ derived from the one-loop decay amplitudes. For the benchmark parameters $\Delta M/M_1 = 10^{-3}\text{--}10^{-5}$ and $\Gamma/M_1 \sim 10^{-6}$, the coherence time of the quasi-degenerate states is much shorter than the timescale of asymmetry generation, so any oscillations in $\epsilon(t)$ are effectively averaged out. Consequently, the time-averaged asymmetry provides an accurate estimate of the integrated baryon yield [36]. Comparisons with quantum-kinetic treatments indicate that deviations from the time-independent approximation remain at the level of at most $\mathcal{O}(10\%)$ in this regime, validating the use of the static approximation for the parameter space considered here.

Flavour effects. Flavour-dependent washout effects can in principle become relevant for $M_{1,2} \lesssim 10^{12} \text{ GeV}$ [37, 38]. However, in the present modular framework, the Yukawa structures yield nearly aligned flavour projectors [39], so the heavy-triplet decays effectively produce a single coherent lepton state. In this case, the total lepton asymmetry is well described by the single-flavour Boltzmann equations employed here. A fully flavour-resolved treatment would primarily redistribute the asymmetry among e, μ, τ flavours and is expected to alter the final baryon asymmetry only at the $\mathcal{O}(1)$ level, without affecting our qualitative co-genesis conclusions.

5 Conclusion

In this work we have presented a unified framework for neutrino masses, baryogenesis, and dark matter based on a modular S_4 symmetry with a type-III seesaw mechanism. The model simultaneously explains the observed neutrino oscillation data and the cosmological baryon and dark matter relic abundances through a common origin in the complex modulus τ , which determines all Yukawa couplings and CP phases.

A detailed numerical analysis was performed for the normal hierarchy of neutrino masses. The modular structure naturally restricts τ to narrow viable bands around $\text{Re } \tau \simeq 1.35$ and 1.64 with $\text{Im } \tau \simeq 2.6\text{--}2.8$, where the modular forms reproduce the observed mixing angles and mass-squared differences within the 3σ ranges of the NuFIT 5.2 (2024) global fit. The framework predicts a nearly maximal leptonic CP phase $\delta_{\text{CP}} \simeq \pm(150^\circ - 180^\circ)$

and an effective Majorana mass $m_{\beta\beta} \simeq (8\text{--}18) \times 10^{-3}$ eV, which lies below the present KamLAND-Zen bound but within the projected sensitivity of nEXO and LEGEND-1000.

The same modular parameter τ that controls the neutrino sector also fixes the Yukawa couplings governing the CP-violating decays of the heavy triplet fermions, thereby linking the visible and dark sectors. The resulting CP asymmetries $|\epsilon_{L,\chi}| \sim 10^{-9}\text{--}10^{-6}$ generate comparable lepton and dark asymmetries through resonant decays of $\Sigma_{1,2}$ at $M_{1,2} \sim 10^7$ GeV. Solutions of the coupled Boltzmann equations show that both asymmetries freeze out with similar magnitudes, yielding the observed baryon asymmetry $\eta_B \simeq 6 \times 10^{-10}$ and the correct dark relic density $\Omega_\chi h^2 \simeq 0.12$ without any parameter tuning.

The co-genesis mechanism exhibits a strong numerical correlation between η_B and $\Omega_\chi h^2$, reflecting the common modular origin of the CP asymmetries. The ratio Ω_χ/Ω_B stabilizes near the cosmological value $3 \lesssim \Omega_\chi/\Omega_B \lesssim 7$, corresponding to a dark-matter mass prediction $m_\chi \simeq 0.1\text{--}2$ GeV. The predicted GeV-scale dark-matter mass and its extremely suppressed interactions with the visible sector ensure full consistency with existing laboratory, astrophysical, and cosmological constraints on asymmetric fermionic dark matter.

The predictive power of the modular S_4 symmetry lies in its ability to relate flavor, CP violation, and cosmology through the single modulus τ . Once τ is fixed by low-energy neutrino data, all other observables—baryon asymmetry, dark matter abundance, and $0\nu\beta\beta$ predictions—follow without additional parameters. This work therefore demonstrates a fully predictive realization of baryon–dark matter co-genesis embedded in a modular flavor theory, linking the origin of flavor and matter–antimatter asymmetry through a common geometric parameter. Future measurements of the leptonic CP phase, neutrinoless double beta decay, and searches for light asymmetric dark matter will provide decisive tests of this unified modular framework.

Appendix A: Essentials of Modular Symmetry and S_4 Yukawa Multiplets

Modular symmetry provides a geometric approach to flavor symmetries in which Yukawa couplings are expressed as modular forms—holomorphic functions of a single complex parameter τ in the upper half-plane ($\text{Im } \tau > 0$). The modulus transforms under the modular group $\text{SL}(2, \mathbb{Z})$ as

$$\tau \longrightarrow \frac{a\tau + b}{c\tau + d}, \quad a, b, c, d \in \mathbb{Z}, \quad ad - bc = 1. \quad (\text{A.1})$$

The two generators,

$$S : \tau \mapsto -\frac{1}{\tau}, \quad T : \tau \mapsto \tau + 1, \quad (\text{A.2})$$

satisfy $S^2 = (ST)^3 = \mathbb{I}$ and define the modular group relations. Finite subgroups $\Gamma_N = \overline{\Gamma}(1)/\overline{\Gamma}(N)$ correspond to well-known discrete flavor symmetries:

$$\Gamma_2 \simeq S_3, \quad \Gamma_3 \simeq A_4, \quad \Gamma_4 \simeq S_4, \quad \Gamma_5 \simeq A_5.$$

In this work we employ $\Gamma_4 \simeq S_4$, the smallest modular group that yields realistic lepton mixing while retaining a nontrivial structure of modular forms.

A modular form of weight k and level N transforms as

$$Y_i(\tau) \longrightarrow (c\tau + d)^k \rho_{ij}(\gamma) Y_j(\tau), \quad \gamma = \begin{pmatrix} a & b \\ c & d \end{pmatrix} \in \Gamma_N, \quad (\text{A.3})$$

where $\rho(\gamma)$ is a unitary representation of the finite modular group. The number of independent modular forms of weight $2k$ increases with N , as summarized in Table 5.

Table 5. Number of linearly independent modular forms of weight $2k$ for low modular levels N .

Level N	Associated group	# of forms (weight $2k$)
2	S_3	$k + 1$
3	A_4	$2k + 1$
4	S_4	$4k + 1$
5	A_5	$10k + 1$

A.1 Structure of the S_4 Group

The finite group S_4 contains five irreducible representations: **1**, **1'**, **2**, **3**, and **3'**. Its generators satisfy

$$S^2 = T^4 = (ST)^3 = \mathbb{I}. \quad (\text{A.4})$$

The relevant Clebsch–Gordan (CG) products are

$$\begin{aligned} 1' \otimes 1' &= 1, & 2 \otimes 2 &= 1 \oplus 1' \oplus 2, & 3 \otimes 3 &= 1 \oplus 2 \oplus 3 \oplus 3', \\ 2 \otimes 3 &= 3 \oplus 3', & 3 \otimes 3' &= 1' \oplus 2 \oplus 3 \oplus 3'. \end{aligned} \quad (\text{A.5})$$

Explicit CG coefficients and representation matrices are listed in Refs. [21, 32] and are used to build modular-invariant Yukawa interactions.

A.2 Modular Forms under S_4

At level $N = 4$, the lowest-weight modular forms furnish a doublet $Y_2^{(2)} = (Y_1, Y_2)^T$ and a triplet-prime $Y_{3'}^{(2)} = (Y_3, Y_4, Y_5)^T$. With $q \equiv e^{2\pi i\tau}$, their schematic q -expansions are

$$\begin{aligned} Y_1 &\simeq 1 + 3q + 3q^2 + \mathcal{O}(q^3), & Y_2 &\simeq \sqrt{3} q^{1/2} (1 + 4q + 6q^2 + \dots), \\ Y_3 &\simeq 1 - 2q + 6q^2 + \dots, & Y_4 &\simeq \sqrt{2} q^{1/4} (1 + 6q + 13q^2 + \dots), \\ Y_5 &\simeq 4\sqrt{2} q^{3/4} (1 + 2q + 3q^2 + \dots). \end{aligned} \quad (\text{A.6})$$

Higher-weight modular multiplets are constructed by modular-covariant products of these basic forms. The independent weight-four combinations used in our model are

$$\begin{aligned} Y_1^{(4)} &= Y_1^2 + Y_2^2, & Y_2^{(4)} &= (Y_2^2 - Y_1^2, 2Y_1Y_2)^T, \\ Y_3^{(4)} &= (-2Y_2Y_3, \sqrt{3}Y_1Y_5 + Y_2Y_4, \sqrt{3}Y_1Y_4 + Y_2Y_5)^T, \\ Y_{3'}^{(4)} &= (2Y_1Y_3, \sqrt{3}Y_2Y_5 - Y_1Y_4, \sqrt{3}Y_2Y_4 - Y_1Y_5)^T. \end{aligned} \quad (\text{A.7})$$

The superscript “(4)” denotes the total modular weight. These multiplets generate all Yukawa couplings appearing in the charged-lepton, neutrino, and dark sectors, ensuring modular-invariant interactions consistent with S_4 representation theory. In practice, only the relative magnitudes and phases of the modular forms—fixed by the chosen value of τ —enter physical observables. The group-theoretical structures, generator matrices, and modular-form expansions presented here follow the conventions established in [44].

Appendix B: Standard Parameterization of Neutrino Observables

The lepton mixing matrix U_{PMNS} is obtained via

$$U_{\text{PMNS}} = U_\ell^\dagger U_\nu, \quad (\text{B.8})$$

where U_ℓ and U_ν diagonalize the charged-lepton and neutrino mass matrices:

$$U_\ell^\dagger M_\ell M_\ell^\dagger U_\ell = \text{diag}(m_e^2, m_\mu^2, m_\tau^2), \quad U_\nu^\dagger M_\nu U_\nu^* = \text{diag}(m_1, m_2, m_3). \quad (\text{B.9})$$

In the PDG convention,

$$U_{\text{PMNS}} = \begin{pmatrix} 1 & 0 & 0 \\ 0 & c_{23} & s_{23} \\ 0 & -s_{23} & c_{23} \end{pmatrix} \begin{pmatrix} c_{13} & 0 & s_{13}e^{-i\delta} \\ 0 & 1 & 0 \\ -s_{13}e^{i\delta} & 0 & c_{13} \end{pmatrix} \begin{pmatrix} c_{12} & s_{12} & 0 \\ -s_{12} & c_{12} & 0 \\ 0 & 0 & 1 \end{pmatrix} P_\nu, \quad (\text{B.10})$$

where $c_{ij} \equiv \cos \theta_{ij}$, $s_{ij} \equiv \sin \theta_{ij}$, and $P_\nu = \text{diag}(1, e^{i\alpha_{21}/2}, e^{i\alpha_{31}/2})$.

Mixing observables follow as

$$\sin^2 \theta_{13} = |U_{e3}|^2, \quad \sin^2 \theta_{12} = \frac{|U_{e2}|^2}{1 - |U_{e3}|^2}, \quad \sin^2 \theta_{23} = \frac{|U_{\mu 3}|^2}{1 - |U_{e3}|^2}, \quad (\text{B.11})$$

and the CP-violating quantities are

$$\delta_{\text{CP}} = -\arg[U_{e1} U_{e3}^* U_{\mu 3} U_{\mu 1}^*], \quad J_{\text{CP}} = \text{Im}[U_{e1} U_{\mu 2} U_{e2}^* U_{\mu 1}^*]. \quad (\text{B.12})$$

The Majorana phases can be expressed as

$$\alpha_{21} = 2 \arg\left(\frac{U_{e2}}{U_{e1}}\right), \quad \alpha_{31} = 2 \arg\left(\frac{U_{e3}}{U_{e1}}\right) + 2\delta_{\text{CP}}. \quad (\text{B.13})$$

The mass-squared splittings and total neutrino mass are

$$\Delta m_{21}^2 = m_2^2 - m_1^2, \quad \Delta m_{31}^2 = m_3^2 - m_1^2, \quad \Sigma m_\nu = m_1 + m_2 + m_3. \quad (\text{B.14})$$

Appendix C: Boltzmann Framework and Scattering Integrals

For completeness, we summarize the Boltzmann equation used in the two-sector analysis. The comoving asymmetries $Y_{\Delta a} = Y_a - Y_{\bar{a}}$ for $a = L, \chi$ evolve according to [8]

$$\begin{aligned} \frac{dY_{\Delta a}}{dz} = & -\frac{\Gamma_{\Sigma_1}}{H_1} \frac{z K_1(z)}{K_2(z)} \left(Y_{\Sigma_1} - Y_{\Sigma_1}^{\text{eq}} \right) \epsilon_a - 2 \text{Br}_a^2 I_W(z) Y_{\Delta a} \\ & - \text{Br}_a \text{Br}_b [I_T^+(z) (Y_{\Delta a} + Y_{\Delta b}) + I_T^-(z) (Y_{\Delta a} - Y_{\Delta b})], \end{aligned} \quad (\text{C.15})$$

where $b \neq a$, $z = M_1/T$, and $H_1 = H(T = M_1)$. The first term describes the CP-violating source from Σ_1 decays, while the remaining terms account for washout and inter-sector transfer effects.

The thermal integrals entering Eq. (C.15) are defined as

$$I_i(z) = \frac{\hat{\Gamma}}{\pi} \int_0^\infty dt t^2 K_1(t) f_i(t^2/z^2), \quad (\text{C.16})$$

where $\hat{\Gamma} = \Gamma_{N_1}/M_{N_1}$, and

$$f_W(s) = \frac{s/2}{(s-1)^2 + \hat{\Gamma}^2} + \frac{s - \log(s+1)}{s} - \frac{2(s-1)}{(s-1)^2 + \hat{\Gamma}^2} \frac{(s+1)\log(s+1) - s}{s} + \frac{s/2}{s+1} + \frac{\log(s+1)}{s+2}, \quad (\text{C.17})$$

$$f_{T^+}(s) = \frac{s/2}{(s-1)^2 + \hat{\Gamma}^2} + \frac{s}{s+1} + \frac{s - \log(s+1)}{s}, \quad (\text{C.18})$$

$$f_{T^-}(s) = \frac{s^2/2}{(s-1)^2 + \hat{\Gamma}^2} + \frac{(s+1)\log(s+1) - s}{s+1} + \frac{(s+2)\log(s+1) - 2s}{s}. \quad (\text{C.19})$$

Here I_W corresponds to $2 \leftrightarrow 2$ washout within a sector, and I_T^\pm encode transfer scatterings between sectors.

As $z = M_1/T$ increases, the pole (on-shell) contributions to the integrals are exponentially suppressed, and inverse decays become subdominant. In this regime, the Boltzmann evolution is controlled by off-shell $2 \leftrightarrow 2$ scattering processes, which admit simple analytic approximations. For $z \gg 1$, the integrals reduce to the asymptotic forms

$$I_D(z) \simeq \frac{3W}{z^2} \frac{H_1}{\Gamma_{N_1}}, \quad I_{T^+}(z) \simeq \frac{W}{z^2} \frac{H_1}{\Gamma_{N_1}}, \quad I_{T^-}(z) \simeq \frac{14W}{z^4} \frac{H_1}{\Gamma_{N_1}}, \quad (\text{C.20})$$

where W denotes the reduced scattering rate.

Appendix D: Behavior of the CP Asymmetry Ratio as a Function of y_{DM}

In order to clarify the origin of the dark-sector dominance observed at small values of y_{DM} , we present in Fig. 12 the ratio $|\epsilon_\chi/\epsilon_L|$ as a function of y_{DM} for a representative benchmark point in the modulus,

$$\tau = 1.64 + i 2.57.$$

For $y_{\text{DM}} \lesssim 10^{-3}$, the ratio exhibits a mild enhancement, arising from the different interference structures entering the visible and dark CP asymmetries. As y_{DM} increases, the ratio smoothly approaches unity, indicating comparable visible and dark contributions. This behavior confirms that the enhancement at small y_{DM} is a controlled quantitative effect rather than a breakdown of the perturbative expansion.

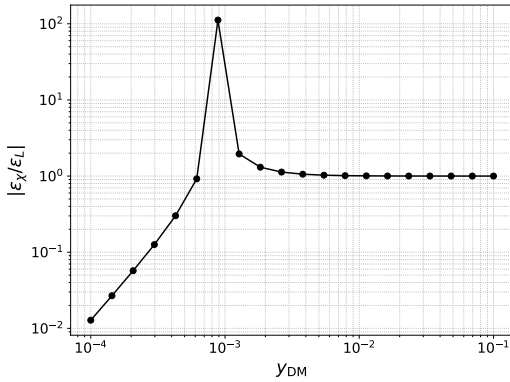


Figure 12. Ratio of CP asymmetries $|\epsilon_\chi/\epsilon_L|$ as a function of the dark Yukawa coupling y_{DM} for a fixed representative value of the modulus $\tau = 1.64 + i 2.57$. The horizontal dashed line indicates equal visible and dark CP asymmetries.

References

- [1] Y. Fukuda *et al.* [Super-Kamiokande Collaboration], “Evidence for Oscillation of Atmospheric Neutrinos,” *Phys. Rev. Lett.* **81** (1998), 1562–1567, doi:10.1103/PhysRevLett.81.1562, arXiv:hep-ex/9807003.
- [2] Q. R. Ahmad *et al.* (SNO Collaboration), “Measurement of the rate of $\nu_e + d \rightarrow p + p + e^-$ and the total active solar neutrino flux,” *Phys. Rev. Lett.* **87** (2001) 071301, 10.1103/PhysRevLett.87.071301, arXiv:nucl-ex/0106015.
- [3] S. Abe *et al.* [KamLAND Collaboration], “Precision Measurement of Neutrino Oscillation Parameters with KamLAND,” *Phys. Rev. Lett.* **100** (2008), 221803, doi:10.1103/PhysRevLett.100.221803, arXiv:0801.4589 [hep-ex].
- [4] N. Aghanim *et al.* (Planck Collaboration), “Planck 2018 results. VI. Cosmological parameters,” *Astron. Astrophys.* **641** (2020) A6, 10.1051/0004-6361/201833910, arXiv:1807.06209.
- [5] V. Abdurashitov *et al.* (DESI Collaboration), “DESI 2024 VI: Cosmological Constraints from the Measurements of Baryon Acoustic Oscillations,” arXiv:2404.03002.
- [6] D. E. Kaplan, M. A. Luty and K. M. Zurek, *Asymmetric dark matter*, *Phys. Rev. D* **79** (2009) 115016, doi:10.1103/PhysRevD.79.115016, arXiv:0901.4117 [hep-ph].
- [7] K. Petraki and R. R. Volkas, *Review of asymmetric dark matter*, *Int. J. Mod. Phys. A* **28** (2013) 1330028, doi:10.1142/S0217751X13300286, arXiv:1305.4939 [hep-ph].
- [8] A. Falkowski, J. T. Ruderman and T. Volansky, *Asymmetric Dark Matter from Leptogenesis*, *JHEP* **05** (2011) 106, doi:10.1007/JHEP05(2011)106, arXiv:1101.4936 [hep-ph].
- [9] B. Dutta and J. Kumar, *Asymmetric dark matter from hidden sector baryogenesis*, *Phys. Lett. B* **699** (2011) 364–367, doi:10.1016/j.physletb.2011.04.036, arXiv:1102.4895 [hep-ph].
- [10] U. Patel, L. Malhotra, S. Patra and U. A. Yajnik, *Cogenesis of visible and dark sector asymmetry in a minimal seesaw framework*, (2022), arXiv:2211.04722 [hep-ph].
- [11] A. Biswas, S. Choubey, L. Covi and S. Khan, *Common origin of baryon asymmetry, dark*

matter and neutrino mass, JHEP **05** (2019) 193, doi:10.1007/JHEP05(2019)193, arXiv:1812.06122 [hep-ph].

- [12] S. Davidson, E. Nardi and Y. Nir, “Leptogenesis,” *Phys. Rept.* **466** (2008) 1–81, 10.1016/j.physrep.2008.06.002, arXiv:0802.2962.
- [13] W. Buchmüller, P. Di Bari and M. Plümacher, *Leptogenesis for pedestrians*, Annals Phys. **315** (2005) 305–351, doi:10.1016/j.aop.2004.02.003, arXiv:hep-ph/0401240.
- [14] M. Fukugita and T. Yanagida, *Baryogenesis Without Grand Unification*, Phys. Lett. B **174** (1986) 45–47, doi:10.1016/0370-2693(86)91126-3.
- [15] A. Pilaftsis and T. E. J. Underwood, “Resonant leptogenesis,” *Nucl. Phys. B* **692** (2004) 303–348, 10.1016/j.nuclphysb.2004.05.021, arXiv:hep-ph/0309342.
- [16] P. S. B. Dev, P. Millington, A. Pilaftsis and D. Teresi, *Resonant Enhancement in Leptogenesis*, Int. J. Mod. Phys. A **33** (2018) 1842003, doi:10.1142/S0217751X18420034.
- [17] J. C. Criado and F. Feruglio, *Modular invariance faces precision neutrino data*, SciPost Phys. **5** (2018) 042, doi:10.21468/SciPostPhys.5.5.042, arXiv:1807.01125 [hep-ph].
- [18] T. Kobayashi and M. Tanimoto, *Modular flavor symmetric models*, (2023), arXiv:2307.03384 [hep-ph].
- [19] T. Kobayashi *et al.*, *A_4 lepton flavor model and modulus stabilization from S_4 modular symmetry*, *Phys. Rev. D*, vol. 100, no. 11, p. 115045, 2019, arXiv:1909.05139. *Erratum: Phys. Rev. D*, vol. 101, p. 039904, 2020.
- [20] J. T. Penedo and S. T. Petcov, *Lepton Masses and Mixing from Modular S_4 Symmetry*, *Nucl. Phys. B*, vol. 939, pp. 292–307, 2019, arXiv:1806.11040.
- [21] X. Wang and S. Zhou, *The minimal seesaw model with a modular S_4 symmetry*, *JHEP*, vol. 05, p. 017, 2020, arXiv:1910.09473.
- [22] R. Foot, H. Lew, X. He and G. C. Joshi, *Seesaw neutrino masses induced by a triplet of leptons*, *Z. Phys. C* **44** (1989) 441, doi:10.1007/BF01548594.
- [23] E. Ma, *Pathways to naturally small neutrino masses*, *Phys. Rev. Lett.* **81** (1998) 1171–1174, doi:10.1103/PhysRevLett.81.1171, arXiv:hep-ph/9805219.
- [24] L. Covi, E. Roulet and F. Vissani, “CP violating decays in leptogenesis: The dominant contribution from self-energy diagrams,” *Phys. Lett. B* **384** (1996) 169–174, 10.1016/0370-2693(96)00814-2, arXiv:hep-ph/9605319.
- [25] A. Falkowski, D. M. Pierce and J. Thaler, “Asymmetric Dark Matter from Hidden Sector Baryogenesis,” *JHEP* **1110** (2011) 028, 10.1007/JHEP10(2011)028, arXiv:1106.3057.
- [26] R. L. Workman *et al.* (Particle Data Group), “Review of Particle Physics,” *PTEP* **2024** (2024) 083C01, 10.1093/ptep/ptad095.
- [27] I. Esteban, M. C. Gonzalez-Garcia, M. Maltoni, I. Martinez-Soler, J. P. Pinheiro and T. Schwetz, *NuFit-6.0: updated global analysis of three-flavor neutrino oscillations*, *JHEP* **12** (2024) 216, doi:10.1007/JHEP12(2024)216
- [28] Abhishek and V. Suryanarayana Mummidi, *Low scale leptogenesis and TM_1 mixing in neutrinoophilic two Higgs doublet model (ν 2HDM) with S_4 flavor symmetry*, *Phys. Lett. B* **870** (2025) 139919, doi:10.1016/j.physletb.2025.139919, arXiv:2504.04413 [hep-ph].
- [29] S. Abe *et al.* [KamLAND-Zen], *Search for Majorana Neutrinos with the Complete KamLAND-Zen Dataset*, (2024), arXiv:2406.11438 [hep-ex].

[30] LEGEND Collaboration, N. Abgrall, I. Abt, et al. LEGEND-1000 Preconceptual Design Report. 2021. arXiv:2107.11462 [physics.ins-det].

[31] G. Adhikari, S. Al Kharusi, E. Angelico, et al. nEXO: neutrinoless double beta decay search beyond 10^{28} year half-life sensitivity. *Journal of Physics G: Nuclear and Particle Physics*, 49(1):015104, 2021. ISSN 1361-6471. DOI: [10.1088/1361-6471/ac3631](https://doi.org/10.1088/1361-6471/ac3631)

[32] P. P. Novichkov, J. T. Penedo, S. T. Petcov and A. V. Titov, *Modular S_4 models of lepton masses and mixing*, JHEP **04** (2019) 005, doi:10.1007/JHEP04(2019)005, arXiv:1811.04933 [hep-ph].

[33] C. S. Fong, M. C. Gonzalez-Garcia, E. Nardi and J. Racker, *Supersymmetric leptogenesis*, JCAP **12** (2010) 013, doi:10.1088/1475-7516/2010/12/013, arXiv:1009.0003 [hep-ph].

[34] M. Flanz, E. A. Paschos and U. Sarkar, “Baryogenesis from a lepton asymmetric decay,” *Phys. Lett. B* **382** (1996) 447–452, 10.1016/0370-2693(96)00698-1, arXiv:hep-ph/9607310.

[35] W. Buchmuller and M. Plumacher, “Status of thermal leptogenesis,” *Phys. Lett. B* **530** (2002) 15–26, 10.1016/S0370-2693(02)01329-5, arXiv:hep-ph/0207189.

[36] T. Garbrecht, “Leptogenesis from first principles in the resonant regime,” *Phys. Rev. D* **90** (2014) 025033, 10.1103/PhysRevD.90.025033, arXiv:1404.3358 [hep-ph].

[37] A. Abada, S. Davidson, A. Ibarra, F.-X. Josse-Michaux, M. Losada and A. Riotto, “Flavour matters in leptogenesis,” *JHEP* **09** (2006) 010, 10.1088/1126-6708/2006/09/010, arXiv:hep-ph/0605281.

[38] E. Nardi, Y. Nir, E. Roulet and J. Racker, “The importance of flavor in leptogenesis,” *JHEP* **01** (2006) 164, 10.1088/1126-6708/2006/01/164, arXiv:hep-ph/0601084.

[39] M. Endo and T. Orikasa, “Leptogenesis in modular symmetry,” *JHEP* **05** (2019) 115, 10.1007/JHEP05(2019)115, arXiv:1812.10709 [hep-ph].

[40] K. M. Zurek, *Asymmetric Dark Matter: Theories, Signatures, and Constraints*, Phys. Rept. **537** (2014) 91–121, doi:10.1016/j.physrep.2013.12.001, arXiv:1308.0338.

[41] F. Feruglio, *Fermion masses, critical behavior and universality*, JHEP **03** (2023) 236, doi:10.1007/JHEP03(2023)236, arXiv:2212.09762 [hep-ph].

[42] S. Mahapatra, P. K. Paul, N. Sahu and P. Shukla, *Asymmetric long-lived dark matter and leptogenesis from the type-III seesaw framework*, Phys. Rev. D **111** (2025) 015043, doi:10.1103/PhysRevD.111.015043, arXiv:2405.00939 [hep-ph].

[43] G. J. Ding, S. F. King, X. G. Liu, and J. N. Lu. Modular S_4 and A_4 symmetries and their fixed points: new predictive examples of lepton mixing. *J. High Energ. Phys.*, 2019(12):030, 2019.

[44] X. Zhang and S. Zhou, Inverse seesaw model with a modular S_4 symmetry: lepton flavor mixing and warm dark matter, arXiv:[2106.03433](https://arxiv.org/abs/2106.03433), 2021.